Thermal analysis on composite girder
with hybrid GFRP-concrete deck

Haohui Xin, Yuqing Liu[*] and Ao Du

Department of Bridge Engineering, Tongji University, Shanghai, China

Abstract. Since the coefficients of thermal expansion (CTE) between concrete and GFRP, steel and GFRP are quite different, GFRP laminates with different laminas stacking-sequence present different thermal behavior and currently there is no specification on mechanical properties of GFRP laminates, it is necessary to investigate the thermal influence on composite girder with stay-in-place (SIP) bridge deck at different levels and on different scales. This paper experimentally and theoretically investigated the CTE of GFRP at lamina's and laminate's level on micro-mechanics scales. The theoretical CTE values of laminas and laminates agreed well with test results, indicating that designers could obtain thermal properties of GFRP laminates with different lamina stacking-sequence through micro-mechanics methods. On the basis of the CTE tests and theoretical analysis, the thermal behaviors of composite girder with hybrid GFRP-concrete deck were studied numerically and theoretically on macro-mechanics scales. The theoretical results of concrete and steel components of composite girder agreed well with FE results, but the theoretical results of GFRP profiles were slightly larger than FE and tended to be conservative at a safety level.

Keywords: composite girder; hybrid GFRP-concrete deck; lamina and laminate's level; coefficients of thermal expansion; thermal multi-scale analysis

1. Introduction

Due to high strength, light weight and non-corrodible nature, fiber reinforced polymer (FRP) composites could be used as main bearing components and strengthening members in the bridge engineering field and have a good application prospect in future bridge construction (Bakis *et al*. 2002, Matta *et al*. 2007). Since FRP composite is inhomogeneous, as shown in Fig.1, FRP composites could be viewed and analyzed theoretically and experimentally at different levels (monomer, lamina and laminate) and on different scales (micro-mechanics and macro-mechanics).

In terms of cost factor in new bridge construction, glass fiber reinforced polymer (GFRP) composites which could meet the established design criteria economically is always recommended. In order to increase flexural stiffness, lower deformation and make the best use of materials, combinations of GFRP laminates and conventional concrete have been adopted (He *et al*. 2012a, Berg *et al*. 2006 and Xin *et al*. 2015).

Recently, lots of research efforts focus on hybrid GFRP-concrete bridge deck, where GFRP

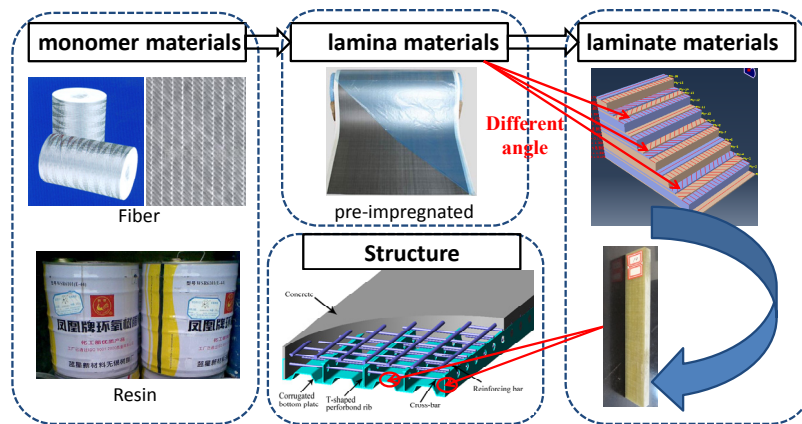*Corresponding author, Ph.D., Professor, E-mail: yql@tongji.edu.cn
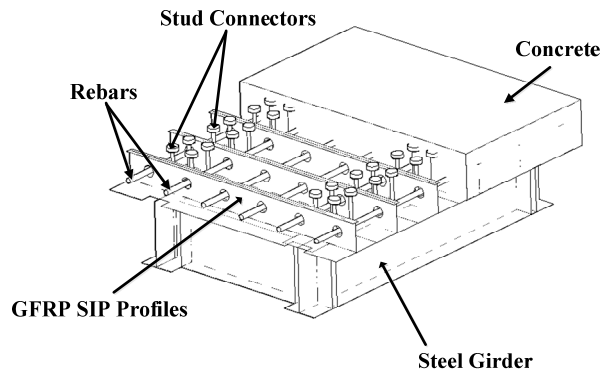
Fig. 1 Three levels of FRP

Fig. 2 Schematic diagram of composite girder with SIP deck

profiles in hybrid structures are used as stay-in-place (SIP) forms to save the construction time and labor cost. As shown in Fig. 2, such composite girder generally consists of steel girder, concrete and GFRP SIP profiles. The GFRP SIP profiles are connected to concrete through holes in T-standup and rebars by forming Perfobond rib shear (PBL) connectors and the hybrid GFRP-concrete decks are connected to steel girder mainly through stud connectors.

Various kinds of SIP bridge deck systems have been designed and studied in the past several decades. The failure modes and fatigue performance were studied and the ultimate and service load were determined based on experiments research by Dieter *et al*. (2002). Bank *et al*. (2006) experimentally studied the mechanical performance of bridge deck with double-layer pultruded FRP grids and presented construction details of the bridge project. Berg *et al*. (2006) combined three forms of FRP reinforcing method (SIP forms, FRP reinforcing bars and FRP reinforcing grid) to propose a new hybrid deck and described the construction process and provided a cost analysis of the highway project. Nelson and Fam (2006) studied the influence width (*w*) of a hybrid deck system relating to spans (s), interface bonding condition, concrete strength and loading location. Full scale deck slab specimens were tested under designed wheel load to investigate the static response, ultimate capacity and failure mechanics by Ringelstetter *et al*. (2006). A type of hybrid FRP-concrete decks consisting of FRP profile with T-upstands or grids as

SIP forms and concrete cast on them was studied by Keller *et al*. (2007) and Schaumann *et al*. (2008). Hanus *et al*. (2008) investigated the mechanical behavior of a hybrid deck for a military prototype bridge subjected to combined bending and compressive axial load. Bank *et al*. (2009) discussed the design and construction specification for SIP form and developed a model for engineers to design and specify such forms. Fam and Nelson (2011) proposed a novel SIP form with pultruded GFRP corrugated plates which were connected together through pin-and-eye connections. He *et al*. (2012a) proposed a novel cost-effective hybrid GFRP and concrete deck, conducted sand filling test and static flexural load tests. Experimental results indicated that the stiffness and strength of GFRP plate under construction load meets the requirements of relative codes. Nelson *et al*. (2013) carried out full bridge test including multiple girders, diaphragms and monolithic connections to evaluate various parameters. Xin *et al*. (2015) experimentally, numerically and theoretically studied the fatigue behavior of hybrid GFRP-concrete bridge decks under sagging moment. The reviewed research work shows high potential for SIP deck system with FRP in tension and concrete in compression and both materials are optimally utilized.

As regard to thermal effects, several researchers investigated the composite girder with GFRP deck panels but few studied composite girder with SIP framework. Reising *et al*. (2004) monitored five-span bridge retrofitted with four different FRP panel systems, the results showed the thermal characteristic of FRP panels are different from those of ordinary reinforced concrete decks, but the consequences caused by these differences are not considered in design process. Kong *et al*. (2013, 2014a) studied thermal field distribution behaviors of a bridge with GFRP sandwich panels and carried out a parametric study to analyze the thermal responses of bridges with different structure combinations. Kong *et al*. (2014b) investigated the thermal behavior of integral abutment bridges with GFRP panels through a numerical study and proposed a homogenization modeling method to analyze GFRP panels under temperature loading effects.

However, since coefficient of thermal expansion (CTE) between concrete and GFRP, steel and GFRP is quite different and the CTE of GFRP is orthotropic, it is significant to investigate the thermal influence on composite girder with hybrid GFRP-concrete deck. Besides, GFRP laminates with different lamina stacking-sequence present different thermal behavior and currently there is no specification on mechanical properties for GFRP laminate. Therefore, it is necessary to investigate the CTE of GFRP laminates at different levels and on different scales.

In order to investigate the thermal effects on composite girder in multi-scale level, the experimental and theoretical analysis on CTE of GFRP laminas and laminates were carried out. On the basis of CTE tests and theoretical analysis, the thermal effects on composite girder were studied based on a three-dimensional finite element (FE) models and theoretical analysis. All the results of experimental, numerical investigations and theoretical analysis in this study may provide reference for the design and construction of such type of bridge.

2. Lamina's CTE

2.1 Fibers and matrix

The mechanical properties and CTE (Soden *et al*. 1998, Ouyang *et al*. 1988, He *et al*. 2012b) of E-glass fibers and epoxy resin are summarized in Tables 1-2. The longitudinal and transverse elastic modulus, poisson's ratio, shear modulus and density of E-glass fiber are 80 GPa, 0.22, 33.33 GPa and 2560 kg/m^3.

Table 1 Mechanical properties of E-glass fibers and epoxy resin

E-glass fibers				
Longitudinal modulus (E_{f1}) /GPa	Transverse modulus (E_{f2}) /GPa	Poisson's ratio (v_f)	Shear modulus (G_f) /GPa	Density (ρ) /(kg/m^3)
80.0	80.0	0.2	33.33	2560
Epoxy resin				
Modulus (E_m) /GPa	Poisson's ratio (v_m)	Shear modulus (G_m) /GPa		Density (ρ) /(kg/m^3)
4.20	0.34	1.57		1160

Table 2 Coefficient of thermal expansion of fiber and matrix under different temperature

Temperature	50°C	70°C	100°C	120°C
Fiber (10^{-6}/°C)	2.16	2.95	2.65	2.53
Matrix* (10^{-6}/°C)	19.0	45.0	62.4	67.1

* Matrix: CTE of matrix at 50°C and 70°C are obtained by linearly extrapolated.

Table 3 Test results for fiber volume fraction

Number	Length (mm)	Width (mm)	Thickness (mm)	Mass before burning (g)	Mass after burning (g)	Composite destiny (kg/m^3)	Fiber fraction (%)
1	24.12	25.11	4.2	4.84	3.65	1902.7	56.1%
2	24.95	23.93	4.05	4.05	3.50	1931.3	56.5%
3	25.00	23.47	4.22	4.22	3.55	1926.4	56.0%
Average						1920.1	56.2%

The elastic modulus, poisson's ratio, shear modulus and density of epoxy resin is 4.20 GPa, 0.38, 1.57 GPa and 1160 kg/m^3. The CTE of E-glass fiber and epoxy resin varies with temperature increasing is shown in Table 2.

2.2 Test for fiber content

Three specimens with layout of 25 mm × 25 mm × 4 mm were fabricated to investigate the fiber fraction based on calcination methods (SAPRC GB/T2577-2005). The specimens were weighed to acquire composite destiny before burning them in the incinerator. After burning (Fig. 3), remaining only consists of fiber and was weighed again to acquire fiber volume fraction. The fiber volume fraction could be obtained based on Eq. (1) (SAPRC GB/T2577-2005). The test results were summarized in Table 3. The average destiny of lamina composite is 1920.1kg/m^3 and the average fiber volume fraction is 56.2%.

$$V_g = \frac{M_f \rho_c}{\rho_f} \tag{1}$$

where M_f is average fiber weight fraction, ρ_c is the density of composite, ρ_f is the density of fiber.

Fig. 3 Specimen after calcination

2.3 Mechanical properties of plies

The engineering constants of a lamina include longitudinal modulus E_1, transverse modulus E_2, shear modulus G_{12}, and Poisson's ratio v_{12}. All could be calculated according to mixture formulae (Jones 1998) as adopted in Eqs. (2)-(7).

$$E_1 = E_{f_1}V_f + E_m V_m \tag{2}$$

$$E_2 = \frac{E_{f_2} E_m \left[V_f + \eta_2 V_m \right]}{E_m V_f + E_{f_2} \eta_2 V_m} \tag{3}$$

$$\eta_2 = \frac{0.2}{1\text{-}v_m}(1.1 - \sqrt{\frac{E_m}{E_f}} + \frac{3.5 E_m}{E_f})(1 + 0.22 V_f) \tag{4}$$

$$G_{12} = \frac{G_f G_m (V_f + \eta_{12} V_m)}{G_m V_f + G_f \eta_{12} V_m} \tag{5}$$

$$\eta_{12} = 0.28 + \sqrt{\frac{E_m}{E_f}} \tag{6}$$

$$v_{12} = v_f V_f + v_m V_m \tag{7}$$

where E_{f1} is longitudinal elastic modulus of fiber, E_{f2} is transverse elastic modulus of fiber, V_f is fiber volume fraction, v_f is Poisson's ratio of fiber, E_m is elastic modulus of matrix, V_m is resin volume fraction, v_m is Poisson's ratio of resin. G_f is shear modulus of fiber, G_m is shear modulus of resin.

2.4 Theory analysis of lamina's CTE

The equation of longitudinal and transverse lamina's coefficient of thermal expansion could be obtained as Eqs. (8)-(9) (Schapery 1968).

$$\alpha_L = \frac{V_f E_{f1}\alpha_{f1} + V_m E_m \alpha_m}{V_f E_{f1} + V_m E_m} \tag{8}$$

$$\alpha_T = V_f(\alpha_{f2} + v_f\alpha_{f1}) + (1+v_m)\alpha_m V_m - (v_f V_f + v_m V_m)\alpha_L \tag{9}$$

where α_L is the thermal expansion coefficient along fiber direction, α_T is the thermal expansion coefficient vertical to fiber direction, α_{f1} is the thermal expansion coefficient of fiber, α_m is the thermal expansion coefficient of matrix.

2.5 Tests for lamina's CTE

Three specimens along fiber directions and three vertical to fiber directions with layout of 50mm×5mm×4mm were (Fig. 4) made to investigate thermal expansion coefficient by PCY High temperature horizontal thermal expansion instrument (Fig. 5). The thermal expansion coefficient could be acquired (SAPRC GB/T2572-2005) as follows

$$\alpha = \frac{\Delta L}{L_0 \Delta t} + \alpha_1 \tag{10}$$

where ΔL is length variation, Δt is temperature amplitude, α_1 is average thermal expansion of equipment's mandril.
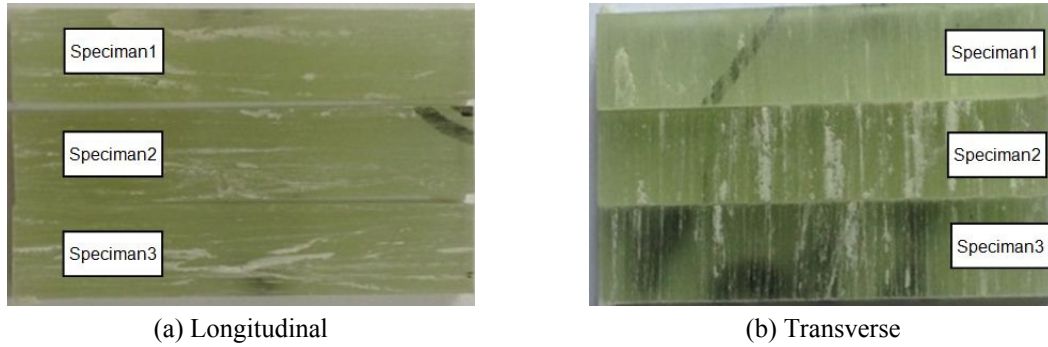

| (a) Longitudinal | (b) Transverse |

Fig. 4 Photo of lamina specimens

Fig. 5 PCY High temperature horizontal thermal expansion instrument
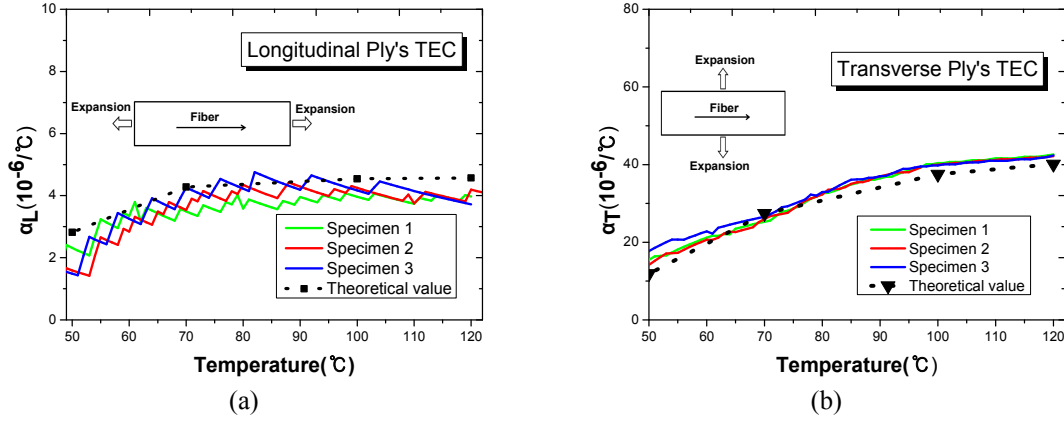
Fig. 6 Lamina's CTE- temperature curve

The relationship between lamina's CTE and temperature is shown in Fig. 6. The longitudinal lamina's CTE increased in the beginning and presented slightly drop after 80°C while the transverse lamina's CTE increased with the temperature increasing but the slop of the curve slightly decreased after 80°C. As is shown in Fig. 6, the lamina's CTE values were predicted based on Eqs. (8)-(9) and the theoretical value agreed well with test results.

3. Laminate's CTE

3.1 Theory analysis of laminate's CTE

The thermal stress resultant in unit length applied on the laminate are denoted by $N^t = \{N_x^t, N_y^t, N_{xy}^t\}^T$, $M^t = \{M_x, M_y^t, M_{xy}^t\}^T$ (Vinson 1999).

$$\{N^t\} = \Delta t \sum_{k=1}^{n} [\bar{Q}]_k \{\bar{\alpha}\}_k (z_k - z_{k-1}) \tag{11}$$

$$\{M^t\} = \frac{\Delta t}{2} \sum_{k=1}^{n} [\bar{Q}]_k \{\bar{\alpha}\}_k (z_k^2 - z_{k-1}^2) \tag{12}$$

$$\{\bar{\alpha}\}_k = \{\bar{\alpha}_1 \quad \bar{\alpha}_2 \quad \bar{\alpha}_{12}\}^T = [T]^T \{\alpha\}_k \tag{13}$$

where $\bar{\alpha}_{12}$ is off-axis thermal expansion coefficient

The stiffness matrix after transformation can be acquired as Eq. (14) based on flexibility matrix $[(S_{ij})]_k$ and transformation matrix $[T]$ (Vinson 1999).

$$[\bar{Q}]_k = [T]^{-1}[(Q_{ij})]_k [T]^{-T} = [T]^{-1}[(S_{ij})]_k^{-1}[T]^{-T} \tag{14}$$

where $\bar{\alpha}_{12}$ is off-axis thermal expansion coefficient

The stiffness matrix after transformation can be acquired as Eq. (14) based on flexibility matrix

$[(S_{ij})]_k$ and transformation matrix $[T]$ (Vinson 1999).

$$[(S_{ij})]_k = \begin{bmatrix} \dfrac{1}{E_1} & -\dfrac{v_{12}}{E_1} & 0 \\ -\dfrac{v_{12}}{E_1} & \dfrac{1}{E_2} & 0 \\ 0 & 0 & \dfrac{1}{G_{12}} \end{bmatrix} \qquad (15)$$

$$\frac{v_{21}}{E_2} = \frac{v_{12}}{E_1} \qquad (16)$$

where the value of E_1, E_2, v_{12} and G_{12} could be acquired by Eqs.(2)-(7).

The transformation matrix [T] (Vinson 1999) can be expressed as follows

$$[T] = \begin{bmatrix} m^2 & l^2 & 2lm \\ l^2 & m^2 & -2lm \\ -lm & lm & m^2 - l^2 \end{bmatrix} \qquad (17)$$

where m is $\cos\theta$, l is $\sin\theta$, θ is angle between fiber direction and principle direction.

The thermal equivalent coefficient of laminate could be acquired based on Eqs. (18)-(19). (Vinson 1999).

$$\{\bar{\alpha}_c\} = \begin{Bmatrix} \bar{\alpha}_{1c} \\ \bar{\alpha}_{2c} \\ \bar{\alpha}_{12c} \end{Bmatrix} = [A]^{-1}[\sum_{k=1}^{n}[T]_k^{-1}(z_k - z_{k-1})]([Q_{ij}]_k\{\alpha\}) \qquad (18)$$

$$A_{ij} = \sum_{k=1}^{n}(\bar{Q}_{ij})_k(z_k - z_{k-1}) \qquad (19)$$

3.2 Tests for laminate's CTE

The laminate lay-up is shown in Fig. 7. The fibers consisted of roving (0^0), axial compound fabric (90^0) and biaxial compound fabric ($\pm 45^0$). The laminates were fabricated by pultrusion method. Two groups and six specimens with 50 mm × 10 mm × 10 mm (Fig. 8) were fabricated to investigate the laminate's CTE (SAPRC GB/T2572-2005).

The relationship between laminates' CTE and temperature load is shown in Fig. 9. The longitudinal laminates' CTE increased from 50°C to 60°C, kept stable at 5.8×10^{-6}/°C from 60°C to 80°C, and then decreased slightly from 80°C to 120°C. The transverse laminates' CTE increased from 50°C to 80°C and dropped from 80°C to 120°C. The decreasing trend of transverse laminates' CTE is larger than longitudinal. The reason is that the CTE of epoxy resin significantly changed after glass transition temperature and the resin volume fraction of transverse direction is larger than longitudinal direction.
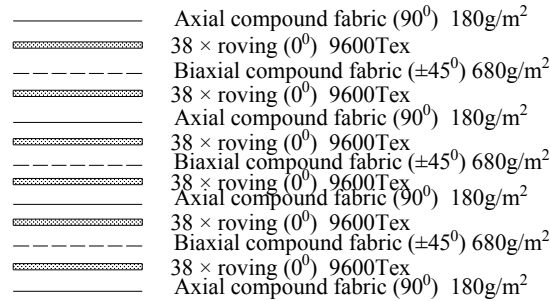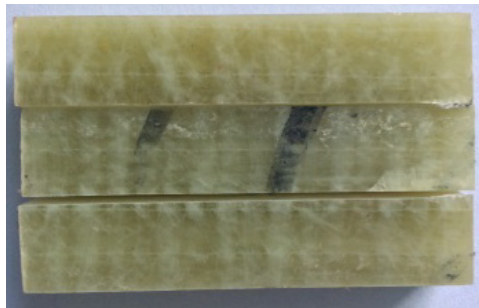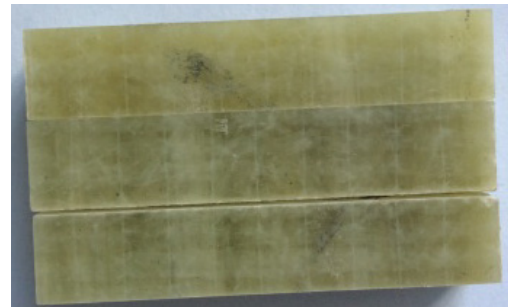
Fig. 7 Laminate lay-up

(a) Longitudinal   (b) Transverse

Fig. 8 Photo of laminate specimens

As is shown in Fig. 9, the laminate's CTE values were predicted based on Eq. (18). The theoretical value of longitudinal laminate's CTE agreed well with test results. The predicted transverse laminate's CTE value also agreed well with test results excepting that the theoretical transverse CTE between 100°C and 120°C were larger than experimental results. One reason is that the axial compound fabric and biaxial compound fabric is assumed to be unidirectional fiber with different angle while the mechanical performance of fabric is different from unidirectional

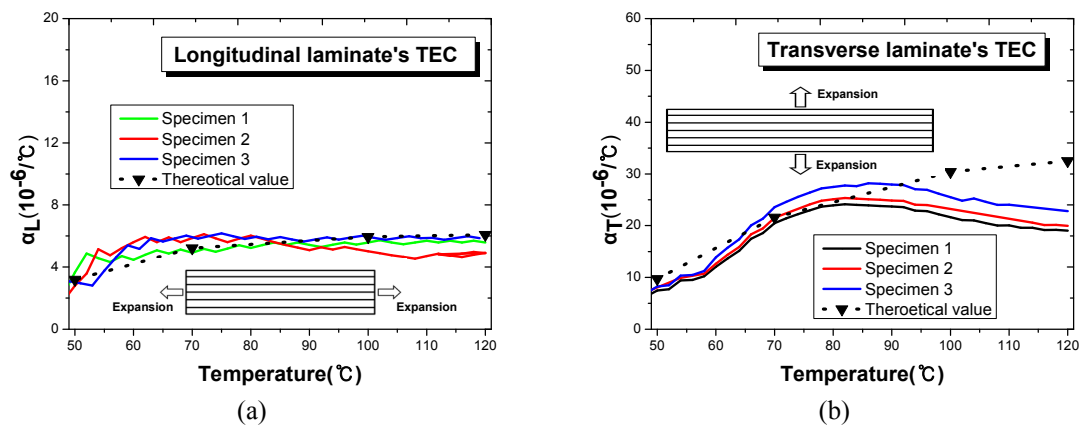(a)   (b)

Fig. 9 Laminate's CTE-temperature curve

fiber. Another reason is that the transverse laminate's CTE related more to the thermal behavior of epoxy resin but the thermal behavior of epoxy resin significantly changed after glass transition temperature (80°C). The predicted results tended to be conservative at a safety side and it will be further investigated in the future study.

4. Thermal effects on composite girder

4.1 Finite element analysis

The modeling of composite girder was carried out by using FE method and software ANSYS (ANSYS Release 11.0), as shown in Fig. 10. Solid elements (SOILID45) were used to simulate concrete deck, GFRP SIP profiles and steel girder. The elastic moduli, Poisson's ratio and CTE of concrete (steel) is 34.5 GPa (210.0 GPa), 0.167(0.3) and $1.0 \times 10^{-5}/°C$ ($1.2 \times 10^{-5}/°C$) based on specification (MTPRC JTC D62). The longitudinal elastic modulus, transverse elastic modulus, longitudinal Poisson's ratio, transverse Poisson's ratio, shear modulus of GFRP laminates is 38.8 GPa, 15.2 GPa, 0.32, 0.13, 5.78 GPa based on previous test results (Xin and Liu 2014). The CTE of longitudinal and transverse GFRP laminate is $0.5 \times 10^{-5}/°C$ and $3.0 \times 10^{-5}/°C$ respectively according to previous section. As for composite action between concrete and steel girder, contact elements (TARGE170 and CONTA173) considering the adhesion effects of steel–concrete interface were employed in FE models and the friction-coefficient is 0.7 (Xin *et al*. 2015). Three spring elements (COMBIN14) for each stud were applied to simulate shear and axial forces in three directions. The shear stiffness of spring element (425.6 kN/mm) is based on experimental results (Lin *et al*. 2014).

The stress distribution of steel, concrete and GFRP SIP profiles is shown in Fig. 11. The concrete all presented tensile stress. The stress of concrete at point A (Fig. 11) showed negative
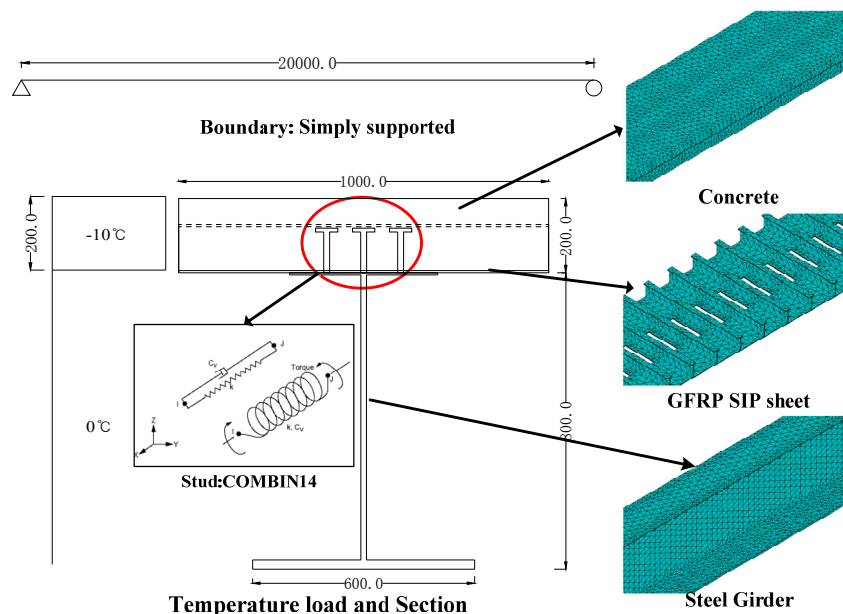

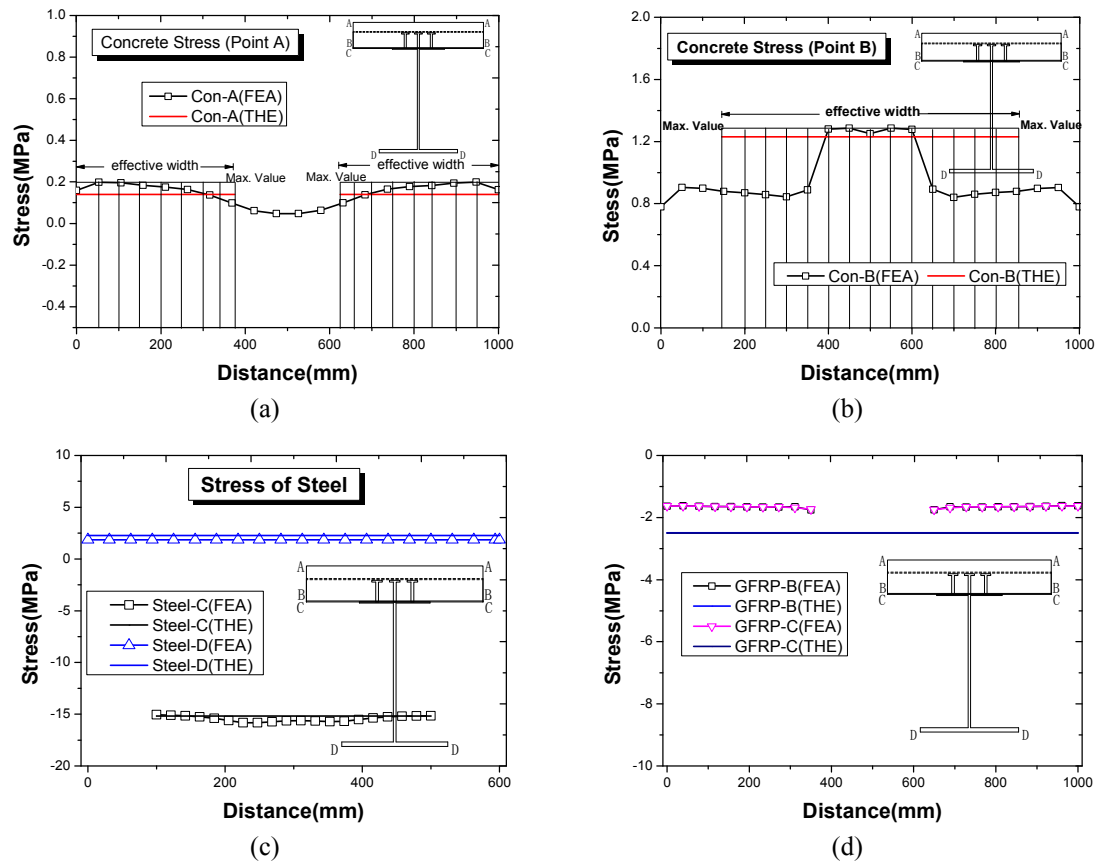Fig. 10 FE model of composite girder with SIP (mm)
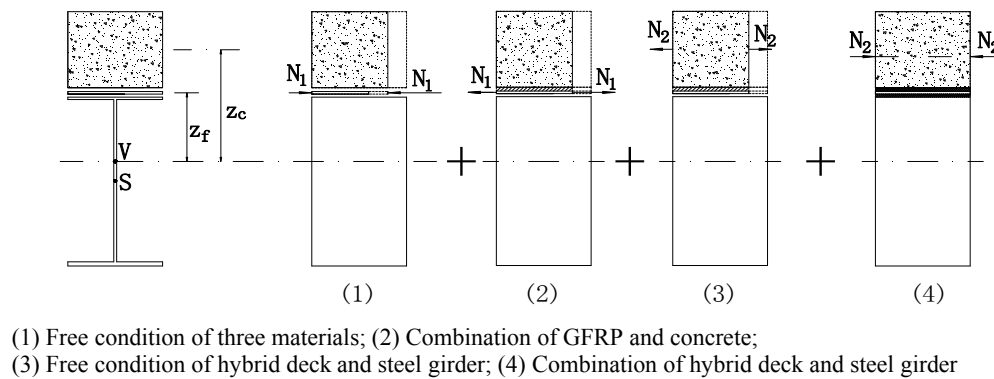
Fig. 11 Strss distribution of each component

(1) Free condition of three materials; (2) Combination of GFRP and concrete;
(3) Free condition of hybrid deck and steel girder; (4) Combination of hybrid deck and steel girder

Fig. 12 Thermal effects analysis of composite girderd

shear lag and the effective width ratio is 0.71 while the stress of concrete at point B (Fig. 11) presented positive shear lag and the effective width ratio is 0.75. The maximum stress of concrete at point A and point B is 0.2 MPa and 1.29 MPa respectively. The stress of upper flange of steel

girder is compressive stress (between -15.0 MPa and -15.9 MPa) while the stress of bottom flange is tensile stress (up to 1.86 MPa). The stress difference at top surface (point B) and at bottom surface (Point C) of GFRP profiles is quite low and the stresses of GFRP profiles are between -1.63 MPa to -1.75 Mpa.

4.2 Theory analysis of thermal effects

As shown in Fig. 12, the thermal analysis was divided into four steps: (1) free condition of three materials; (2) Combination of GFRP profiles and concrete; (3) Free condition of hybrid deck and steel girder; (4) Combination of hybrid deck and steel girder.

If steel girder, concrete and GFRP are free, the concrete and FRP will freely expand due to thermal effects. The equivalent force N_1 and N_2 could be calculated as Eqs. (20)-(21) by applying force which could make concrete and GFRP original.

$$N_1 = \left(\alpha_f - \alpha_c\right)\Delta t E_f A_f \tag{20}$$

$$N_2 = \alpha_c \Delta t \left(E_f A_f + E_c A_c\right) \tag{21}$$

where, α_f is CTE of GFRP, α_c is CTE of concrete, Δt is temperature amplitude, E_c is elastic modulus of concrete, E_f is elastic modulus of GFRP, A_f is area of GFRP, A_c s area of concrete.

If it is the free condition for three materials, the stress of GFRP (σ_{f1}) in the first condition could be acquired as follows

$$\sigma_{f1} = \left(\alpha_f - \alpha_c\right)\Delta t E_f \tag{22}$$

As shown in Fig. 13, if it is just the combination of GFRP and concrete, the stress of GFRP and concrete (σ_{c2}^A and σ_{c2}^B) in the second condition could be acquired by Eqs. (23)-(27).

$$M_1 = N_1 e_1 \tag{23}$$

$$\sigma_{c2}^A = \frac{N_1}{A_{deck}} - \frac{M_1 y_1}{I_{deck}} \tag{24}$$

$$\sigma_{c2}^A = \frac{N_1}{A_{deck}} - \frac{M_1 y_1}{I_{deck}} \tag{25}$$

$$\sigma_{f2}^B = \frac{1}{n_f}\left(\frac{N_1}{A_{deck}} + \frac{M_1 y_2}{I_{deck}}\right) \tag{26}$$

$$\sigma_{f2}^C = \frac{1}{n_f}\left(\frac{N_1}{A_{deck}} + \frac{M y_3}{I_{deck}}\right) \tag{27}$$

where e_1, y_1, y_2 and y_3 is corresponding distance (as shown in Fig. 13), A_{deck} is equivalent area of deck, I_{deck} is equivalent moment of inertia of deck considering shear lag effects (The property of hybrid deck is calculated with effective width), n_f is the ratio between E_f and E_c.
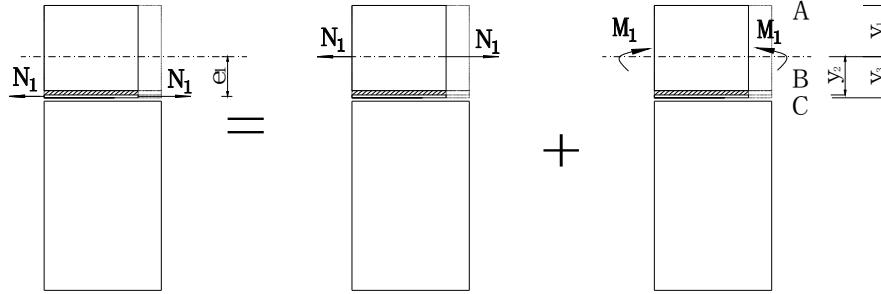
Fig. 13 Stress distribution during Combination of GFRP and concrete

If it is the free condition of hybrid deck and steel girder, the stress of GFRP (σ_{f3}) and concrete (σ_{c3}) in third condition could be acquired by Eqs. (28)-(29).

$$\sigma_{f3} = \alpha_c \Delta t \, E_f \tag{28}$$

$$\sigma_{c3} = \alpha_c \Delta t \, E_c \tag{29}$$

As shown in Fig. 14, the stress of GFRP (σ_{f4}^B and σ_{f4}^C), concrete (σ_{c4}^A and σ_{c4}^B) and steel (σ_{s4}^C and σ_{s4}^D) in the fourth condition could be calculated by Eqs. (30)-(36).

$$M_2 = N_2 e_2 \tag{30}$$

$$\sigma_{c4}^A = -\frac{N_2}{A_{girder}} - \frac{M_2 z_1}{I_{girder}} \tag{31}$$

$$\sigma_{c4}^B = -\frac{N_2}{A_{girder}} - \frac{M_2 z_2}{I_{girder}} \tag{32}$$

$$\sigma_{f4}^B = -\frac{1}{n_f}\left(\frac{N_2}{A_{girder}} + \frac{M_2 z_2}{I_{girder}}\right) \tag{33}$$

$$\sigma_{f4}^C = -\frac{1}{n_f}\left(\frac{N_2}{A_{girder}} + \frac{M_2 z_3}{I_{girder}}\right) \tag{34}$$

$$\sigma_{s4}^C = -\frac{1}{n_s}\left(\frac{N_2}{A_{girder}} + \frac{M_2 z_3}{I_{girder}}\right) \tag{35}$$

$$\sigma_{s4}^D = -\frac{1}{n_s}\left(\frac{N_2}{A_{girder}} - \frac{M_2 z_4}{I_{girder}}\right) \tag{36}$$

where e_2, z_1, z_2, z_3 and z_4 is corresponding distance (Fig. 14); A_{girder} is equivalent area of composite girder; I_{girder} is equivalent moment of inertia of composite girder considering shear lag effects (The
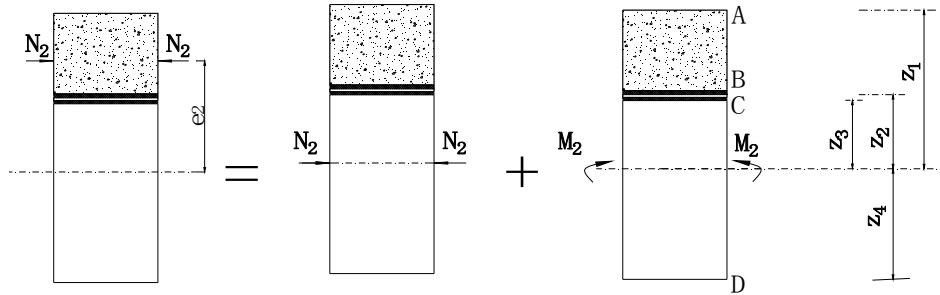
Fig. 14 Stress distribution during Combination of hybrid deck and steel girderd

property of hybrid deck is calculated with effective width); n_s is the ratio between elasticity modulus of steel E_s and E_c.

Thus, the final stress of concrete (σ_c^A and σ_c^B) GFRP (σ_f^B and σ_f^C), and steel (σ_s^C and σ_s^D) in the fourth condition could be acquired as follows

$$\sigma_c^A = \sigma_{c2}^A + \sigma_{c3} + \sigma_{c4}^A \tag{37}$$

$$\sigma_c^B = \sigma_{c2}^B + \sigma_{c3} + \sigma_{c4}^B \tag{38}$$

$$\sigma_f^B = \sigma_{f1} + \sigma_{f2}^B + \sigma_{f3} + \sigma_{f4}^B \tag{39}$$

$$\sigma_f^C = \sigma_{f1} + \sigma_{f2}^C + \sigma_{f3} + \sigma_{f4}^C \tag{40}$$

$$\sigma_s^C = \sigma_{s4}^C, \quad \sigma_s^D = \sigma_{s4}^D \tag{41}$$

4.3 Comparison of FE and theoretical results

The theoretical results are shown in Fig. 11. Due to shear lag effects, the stress of concrete near the web may be larger or smaller than other places. The stress distribution is always simplified as a rectangle with maximum stress and effective width in a safety side. The theoretical results of concrete agreed well with the maximum stress of FE results indicating the theoretical results could be used in the practical engineering. The theoretical results of upper flanges and bottom flanges of steel girder also agreed well with FE results, but the theoretical results of GFRP were larger than FE and tended to be conservative at a safety level.

5. Conclusions

This paper investigated the CTE of GFRP at both lamina's and laminate's level experimentally and theoretically. On the basis of the CTE test results and theoretical analysis, the thermal behavior of composite girder with hybrid GFRP-concrete deck is studied through a three-dimensional FE models and theoretical analysis. The following conclusions can be drawn from the present study:

- The tests showed the longitudinal lamina's CTE increased in the beginning and presented slightly fall after 80°C while the transverse lamina's CTE increased with the temperature increasing. The transverse lamina's CTE is ten times larger than the longitudinal lamina's CTE. The theoretical value of lamina's CTE based on micromechanics of composites agreed well with test results.
- The tests showed the longitudinal lamina's CTE increased in the beginning and presented slightly fall after 80°C while the transverse lamina's CTE increased with the temperature increasing. The transverse lamina's CTE is ten times larger than the longitudinal lamina's CTE. The theoretical value of lamina's CTE based on micromechanics of composites agreed well with test results.
- The theoretical results of concrete and steel component of composite girder agreed well with FE results, but the theoretical results of GFRP were larger than FE and tended to be conservative at a safety level.

Acknowledgments

References

ANSYS (2005), Release 11.0; ANSYS University Advanced, ANSYS Inc.

Bakis, C.E., Bank, L.C., Brown, V.L., Cosenza, E., Davalos, J.F., Lesko, J.J., Machida, A., Rizkalla, S.H. and Triantafillou, T.C. (2002), "Fiber-reinforced polymer composites for concstruction – state-of-art-review", *J. Compos. Construct.*, **6**(2), 73-88.

Bank, L.C., Oliva, M.G., Russell, J.S., Jacobson, D.A., Conachen, M., Nelson, B. and McMonigal, D. (2006), "Double-layer prefabricated FRP grids for rapid bridge deck construction: Case study", *J. Compos. Construct.*, **10**(3), 204-212.

Bank, L.C., Malla, A.P., Oliva, M.G., Russell, J.S., Bentur, A. and Shapira, A. (2009), "A model specification for fiber reinforced non-participating permanent formwork panels for concrete bridge deck construction", *Construct. Build. Mater.*, **23**(7), 2664-2677.

Berg, A.C., Bank, L.C., Oliva, M.G. and Russell, J.S. (2006), "Construction and cost analysis of an FRP reinforced concrete bridge deck", *Construct. Build Mater.*, **20**(8), 515-526.

Dieter, D.A., Dietsche, J.S., Bank, L.C., Oliva, M.G. and Russell, J.S. (2002), "Concrete bridge decks constructed with fiber-reinforced polymer stay-in-place forms and grid reinforcing", *Transport. Res. Rec.*, **1814**, 183-189.

Fam, A. and Nelson, M. (2011), "New bridge deck cast onto corrugated GFRP stay-in-place structural forms with interlocking connections", *J. Compos. Construct.*, **16**(1), 110-117.

Hanus. J.P., Bank. L.C. and Oliva, M.G. (2008), "Combined loading of a bridge deck reinforced with a structural FRP stay-in-place form", *Constcut. Build Mater.*, **23**(4), 605-1619.

He, J., Liu, Y.Q., Chen, A.R. and Dai, L. (2012a), "Experimental investigation of movable hybrid GFRP and concrete bridge deck", *Construct. Build Mater.*, **26**(1), 49-64.

He, Y.X., Zhang, L., Zhu, S.B., Yao, D.H., Zhang, Z.Q. and Zhang, Y.Q. (2012b), "Effect of core-shell polymer particles on the coefficient of thermal expansion epoxy resin", *Thermosetting Resin*, **27**(1), 5-8. [In Chinese]

Jones, R.M. (1998), *Mechanics of Composite Materials*, Taylor & Francis Inc., Oxfordshire, UK.

Keller, T., Schaumann, E. and Vallée, T. (2007), "Flexural behavior of a hybrid FRP and lightweight concrete sandwich bridge deck", *Compos. Part A-APPL. S*, **38**(3), 879-889.

Kitane, Y., Aref, A.J. and Lee, G.C. (2004), "Static and fatigue testing of hybrid fiber-reinforced polymer-concrete bridge superstructure", *J. Compos. Construct.*, **8**(2), 182-190.

Kong, B., Cai, C.S. and Kong, X. (2013), "Thermal behaviors of concrete and steel bridges after slab replacements with GFRP honeycomb sandwich panels", *Eng. Struct.*, **56**, 2041-2051.

Kong, B., Cai, C.S. and Pan, F. (2014a), "Thermal field distributions of girder bridges with GFRP panel deck versus concrete deck", *J. Bridge Eng.*, **19**(11), 04014046.

Kong, B., Cai, C.S. and Kong, X. (2014b), "Thermal property analysis and applications of GFRP panels to integral abutment bridges", *Eng. Struct.*, **76**, 1-9.

Lin, Z.F., Liu, Y.Q. and He, J. (2014), "Behavior of stud connectors under combined shear and tension loads", *Eng. Struct.*, **81**, 362-376.

Matta, F., Nanni, A. and Bank, L.C. (2007), "Prefabricated FRP reinforcement for concrete bridge deck and railing: Design, laboratory validation and field implementation", *Proceedings of Asia-Pacific Conference on FRP in Structures* (*APFIS2007*), Hong Kong, December.

Ministry of Transport of the People's Republic of China (MTPRC JTC D62) (2004), Code for design of highway reinforced concrete and prestressed concrete bridges and culverts; Beijing, China. [In Chinese]

Nelson, M. and Fam, A. (2006), "Full bridge testing at scale constructed with novel FRP stay-in-place structural forms for concrete deck", *Construct. Build Mater.*, **50**, 368-376.

Nelson, M., Eldridge, A. and Fam, A. (2013), "The effects of splices and bond on performance of bridge deck with FRP stay-in-place forms at various boundary conditions", *Construct. Build Mater.*, **56**, 509-516.

Ouyang, G.N., Xu, L., Liu, C.M. and Xu, J. (1988), "Experimental study on the coefficient of thermal expansion for several fibers", *Aerosp. Mater. Technol.*, **04**, 48-53. [In Chinese]

Reising, R.M., Shahrooz, B.M., Hunt, V.J., Neumann, A.R. and Helmicki, A.J. (2004), "Performance comparison of four fiber-reinforced polymer deck panels", *J. Compos. Construct.*, **8**(3), 265-274.

Ringelstetter, T.E., Bank, L.C., Oliva, M.G., Russell, J.S., Matta, F. and Nanni, A. (2006), "Structural stay-in-place formwork system of fiber - Reinforced polymer for accelerated and durable bridge deck construction", *Transport. Res. Rec.*, **1976**, 219-226.

Schapery, R.A. (1968), "Thermal expansion coefficients of composite materials based on energy principles", *J. Compos. Mater.*, **2**(3), 380-404.

Schaumann, E., Vallée, T. and Keller, T. (2008), "Direct load transmission in hybrid FRP and lightweight concrete sandwich bridge deck", *Compos. Part A-APPL. S*, **39**(3), 478-487.

Standardization Administration of the People's Republic of China (SAPRC GB/T2577-2005) (2005), Test method for resin content of glass fiber reinforced plastics; SAPRC, Beijing, China. [In Chinese]

Standardization Administration of the People's Republic of China (SAPRC GB/T2572-2005) (2005), Fiber-reinforced plastics composites — Determination for mean coefficient of linear expansion; SAPRC, Beijing, China. [In Chinese]

Soden, P.D., Hinton, M.J. and Kaddour, A.S (1998), "Lamina properties, lay-up configurations and loading conditions for a range of fibre-reinforced composite laminates", *Compos. Sci. Technol.*, **58**(7), 1011-1022.

Vinson, J.R. (1999), *The Behavior of Sandwich Structures of Isotropic and Composite Materials*, Technomic Publishing Co., PA, USA.

Xin, H.H. and Liu, Y.Q. (2014), "Material tests on pultruded glass fiber reinforced polymer (GFRP) profiles for bridge structures", *The 1st Joint Workshop on Building / Civil Engineering between Tongji university and Tokyo Institute of Technology*, Tokyo, Japan, August. DOI: 10.13140/2.1.4550.0805

Xin, H.H., Liu, Y.Q., He, J., Fan, H.F. and Zhang, Y.Y. (2015), "Fatigue behavior of hybrid GFRP-concrete bridge decks under sagging moment", *Steel Compos. Struct.*, *Int. J.*, **18**(5), 925-946.

CC